2.1 A 0.24nJ/b Wireless Body-Area-Network Transceiver with Scalable Double-FSK Modulation

Joonsung Bae, Kiseok Song, Hyungwoo Lee, Hyunwoo Cho, Long Yan, Hoi-Jun Yoo

KAIST, Daejeon, Korea

Wireless Body Area Network (WBAN) is an emerging technology that combines health care and consumer electronic applications around the human body. There are 3 PHY schemes discussed in the IEEE 802.15.6 Task Group for WBAN standardization [1]: ultra-wide-band (UWB) PHY, narrow-band (NB) PHY, and body channel communication (BCC) PHY. The BCC, which uses the human body as a communication channel based on the near-field coupling mechanism, has advantages over UWB and NB in energy efficiency because it provides low path-loss without the body shadowing effect in low-frequency bands below 150MHz [2-4]. However, the previous body channel transceivers (BCTs) were not optimized for WBAN because only phenomenological circuit models were used for the body channel analysis [5] and were unable to satisfy requirements such as energy efficiency, scalability of QoS, interference mitigation, and coexistence at once.

In this paper, we report a BCT that not only consumes the lowest energy with very high sensitivity but also is fully WBAN compatible. It is possible because: (1) the signal propagation principle is more thoroughly investigated, (2) resonance matching (RM) and context-aware sensing (CAS) are adopted, and (3) low-power double-FSK modulation is exploited for the full satisfaction of WBAN requirements.

According to the experimental data, a BCC signal path can be divided into 2 parts: forward path, and return path as shown in Fig. 2.1.1. Electrodes in contact or in close proximity to the human body constitute the forward path while the floated ground electrodes of TX and RX form the closed-loop return path by capacitive-coupling to the earth ground. The signal path loss has band-pass characteristics, mainly determined by the return path loss because the small capacitance of C_R in the return path has the highest impedance value compared with the contact impedance (electrode-to-body) and body impedance. RM cancels the C_R effect by inserting a resonating series inductor in the return path. The contact impedance in the forward path varies its value dynamically and even 30dB overall signal path loss variation is observed when the electrode is in contact with or apart from the body. To compensate for channel quality degradation due to contact impedance variation, the CAS observes the contact impedance by recognizing if the electrode is capacitively coupled or resistively coupled to the human body, and then automatically determines the BCT operation mode for the better power efficiency.

Figure 2.1.2 shows the overall architecture of the BCT using scalable double-FSK, which is based on UWB-FM [6]. The BCC uses a 40-to-120MHz frequency band while the CAS utilizes a chopper-stabilized AC current-injection source of 1MHz to monitor the differential contact impedance between 2 electrodes. On the TX side, from the frequency synthesizer and divider chain, a low-modulation-index sub-band FSK signal S(t) is transformed into a high-modulation-index wide-band FSK signal W(t) that drives the electrodes. On the RX side, the delay-line-based wide-band demodulator converts the RF carrier signal into a sub-band FSK signal that is demodulated by low-frequency direct-conversion RX circuits. Combined with RM and CAS, the double-FSK BCT has 3 low-power features: reconfigurable differential LNA/driver, current-reuse wide-band demodulator, and divider-based LO generation with duty-cycle corrector (DCC), which together reduce the power consumption by half.

Figure 2.1.3 shows the fully differential reconfigurable LNA of RX and TX driver with RM scheme. The dual-resonance networks at GND electrodes are matched over a wide frequency range between RX and TX. As a result, RM in both TX and RX enhances the return signal path by 4dB as shown in Fig. 2.1.3. The capacitively cross-coupled common-gate LNA in RX provides low impedance to the series RM network and balances the RF signal gain between differential inputs. Moreover, the noise figure (3 to 16dB), input referred 1dB compression point (-18 to -6dBm), and gain (13 to 22dB) of the LNA can be adjusted by controlling the size of M_1 and M_2 with constant bias current. In contrast, the inverter-based TX driver provides a high impedance to effectively drive the parallel RM network. The voltage swing of TX output, from 1 to 6V, controlled by a 5b digital code, can be also modified at 50Ω load to increase its power efficiency.

The wide-band FSK demodulator simultaneously demodulates multiple signals even though the received signal has a negative SNR. A fixed time delay with Gilbert-multiplier is adopted for wide-band FSK demodulation as shown in Fig. 2.1.4. To reduce power, the bias current of I_B is shared between the Gilbert multiplier and current-driven lattice all-pass filter. The delayed signal from M_1 and lattice LC tank is fed to sources of M_2 and M_3, where it is multiplied with the non-delayed signal, yielding the low-frequency sub-band signal at the output. To avoid frequency offset in demodulation, the frequency at the phase shift of $\pi/2$ is modified by controlling C_{tune} with a varactor. Similarly, to ensure a linear group delay in the operating frequency range, a variable MOS resistor, R_{tune}, is added. The output of the demodulator is obtained by a 1Mb/s FM signal with -40dBm RF input power.

Since the sub-band signal is located in a low frequency band below 20MHz, the reference clock is divided to obtain a sub-band LO signal without using a high-power frequency synthesizer. The output of the divider chain must have an exact 50% duty cycle to generate an accurate I/O signal. However, the LO signal generated by a pulse swallow-based programmable divider cannot guarantee 50% duty cycle due to the prescaler operation. To ensure 50% duty cycle, the DCC circuit is implemented as in Fig. 2.1.5(a). The complementary charge-pump circuits detect the imbalance in the duty cycle of CLK_{OUT} and convert it into the mismatch between I_{C1} and I_{C2}. This mismatch is regulated to be equal by DCC loop gain for the duty-cycle correction. When 11% duty-cycle signal, which is generated by /23 using a pulse swallow divider, is applied to DCC, CLK_{OUT} is improved up to 50% duty cycle while consuming 80μW.

Figure 2.1.5(b) shows the micrograph of the WBAN transceiver. It is fabricated in 0.18μm CMOS and its area is 2.5×5mm² including pads. The scalable double-FSK signals are modulated from 4 sub-bands with variable data rate of 10kb/s to 10Mb/s and its TX output spectra are shown in Fig. 2.1.6. Each sub-band is distinguished by a wide-band FSK demodulator with corresponding sub-band carrier frequencies. To demonstrate WBAN coexistence in a low-SNR condition, 2 users that occupy the same sub-band (2MHz) with different sub-band carrier frequencies of 0.5MHz and 1MHz are applied with -40dBm RF input. The time-domain waveforms show the output of the wide-band demodulator using the RF inputs of 2 users. The performance and comparisons of Fig. 2.1.7 shows that the BCT supports all requirements for WBAN in terms of sensitivity, data rate, scalable BER, interference rejection, and co-existence thanks to scalable double-FSK modulation. The RM and CAS reduce the power consumption of the LNA and TX driver. In addition, the bias-reuse wide-band demodulator, and divider-based LO generation with DCC make the power-hungry frequency synthesizer unnecessary. As a result, the RX consumes 2.4mW with a data rate of 10Mb/s. Its minimum detectable signal is 250μV, which is 80× better than [2]. The energy consumption is 0.24nJ/b, which is the most energy efficient among the reported BCTs in our table.

References:

[1] IEEE 802.15 WPAN™ Task Group 6: Body Area Networks (BAN), Nov. 2007 [Online]. Available: http://www.ieee802.org/15/pub/TG6.html

[2] S. Song, et al., "A 0.9V 2.6mW Body-Coupled Scalable PHY Transceiver for Body Sensor Applications," *ISSCC Dig. Tech. Papers*, pp. 366-367, Feb. 2007.

[3] N. Cho, et al., "A 60kb/s-to-10Mb/s 0.37nJ/b Adaptive-Frequency-Hopping Transceiver for Body-Area Network," *ISSCC Dig. Tech. Papers,* pp. 132-133, Feb. 2008.

[4] A. Fazzi, et al., "A 2.75mW Wideband Correlation-Based Transceiver for Body-Coupled Communication," *ISSCC Dig. Tech. Papers,* pp. 204-205, Feb. 2009

[5] N. Cho, et al., "The Human Body Characteristics as a Signal Transmission Medium for Intrabody Communication," *IEEE Trans. Microwave Theory and Techniques*, vol. 55, pp. 1080-1086, May. 2007.

[6] J. Gerrits, et al., "Principles and Limitations of Ultra-Wideband FM Communications Systems," *EURASIP J. Applied Signal Processing,* vol. 2005, no. 3, pp. 382-396, Mar. 2005.

 978-1-61284-302-5/11/$26.00

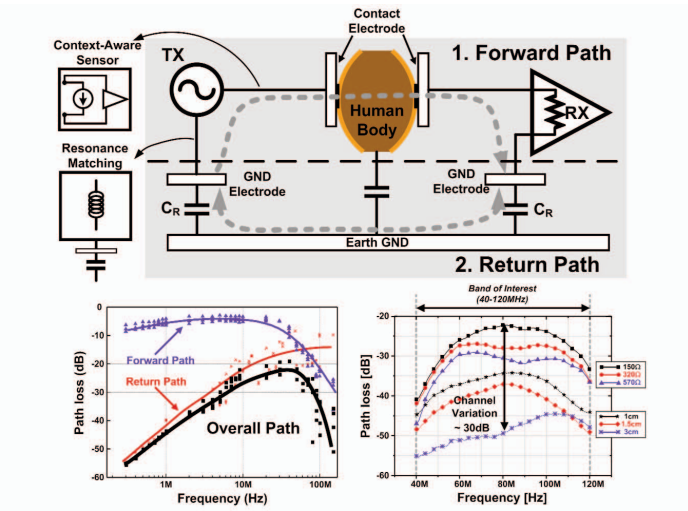

Figure 2.1.1: BCC propagation principle.

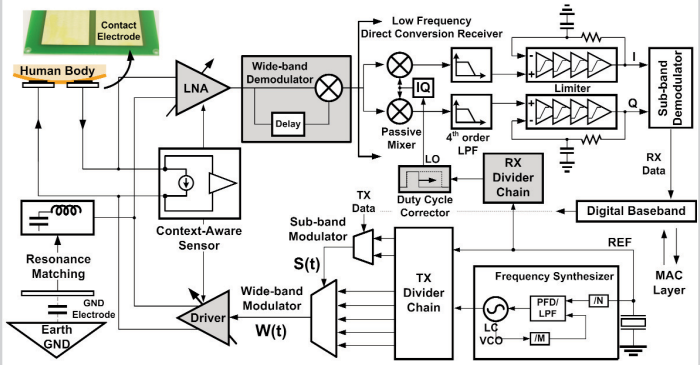

Figure 2.1.2: Overall architecture of the BCT.

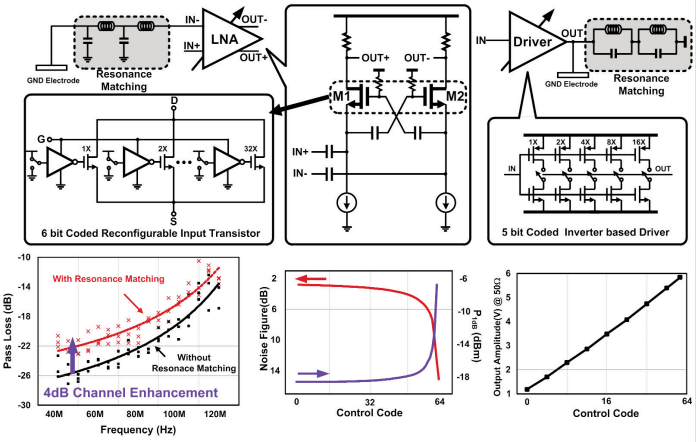

Figure 2.1.3: Reconfigurable LNA and TX driver with resonance matching.

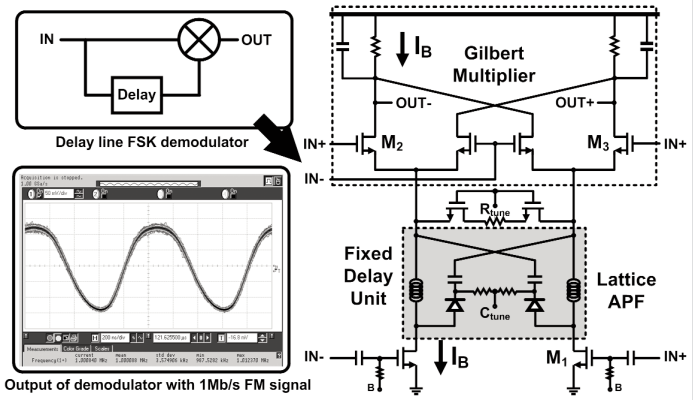

Figure 2.1.4: Bias-reuse wide-band FSK demodulator.

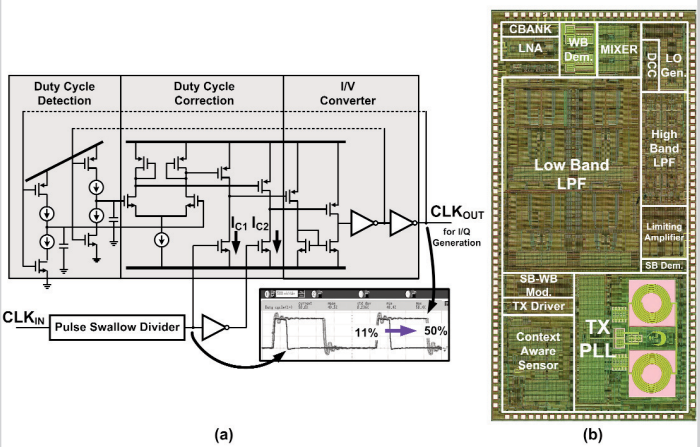

Figure 2.1.5: (a) Duty cycle corrector (b) Chip micrograph.

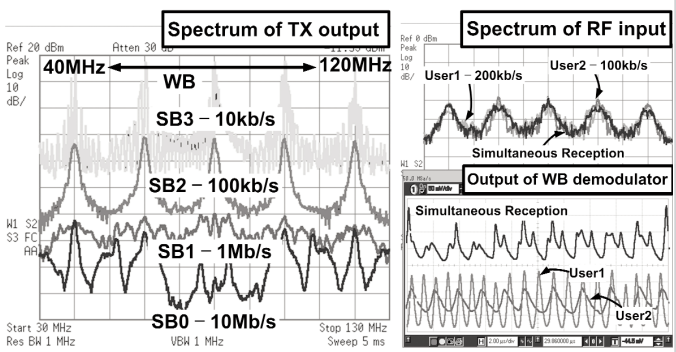

Figure 2.1.6: Measurement results of the double-FSK BCT.

Technology		0.18 μm RF CMOS
Die Area		2.5mm X 5mm
Frequency Band		40 MHz - 120 MHz
Modulation		FSK - FSK (Double FSK)
LNA Gain		13 to 22 dB
Post LNA Amp. Gain		0 to 30 dB
Sensitivity		-66 to -40 dBm
Data Rate		10 Mb/s to 1kb/s
BER @ -62dBm		10^{-5} @ 10Mb/s & 10^{-12} @ 10kb/s
Interference Rejection		6 to 36 dB
# of Co-existence		1 to 15
Supply Voltage		1.0 V
Power Break-down	Transmitter	
	TX PLL	1.0 mW
	Divider/Other	0.8 mW
	Driver	0.2 to 2.0 mW
	Total	2.0 to 3.8 mW
	Receiver	
	LNA	0.6 mW
	Post LNA Amp.	0 to 0.8 mW
	WB Demdulator	0.4 mW
	LP Filter X 2	0.4 X 2 mW
	Limitter X 2	0.2 X 2 mW
	DCC & CAS	0.1 mW
	Divider/Other	0.1 mW
	Total	2.4 to 3.2 mW
Energy/bit		0.24nJ/b

Parameters	ISSCC 2007 [2]	ISSCC 2008 [3]	ISSCC 2009 [4]	This Work
Technology	0.18μm CMOS	0.18μm CMOS	0.13μm CMOS	0.18μm CMOS
Supply Voltage	0.9V	1V	1.2V	1V
Modulation	3-Level PPM	AFH FSK	Correlation Direct Digital	Double FSK
Frequency Band	10-70MHz	30-120MHz	1-30MHz	40-120MHz
Data Rate	10kb/s - 10Mb/s	60kb/s - 10Mb/s	8.5Mb/s	1kb/s - 10Mb/s
Sensitivity	-30dBm	-65dBm	-60dBm	-66dBm
# of Coexistence	128	1	1	15
Power Consumption	2.6mW	3.7mW	2.75mW	2.4mW
Energy/bit	0.26nJ/b	0.37nJ/b	0.32nJ/b	0.24nJ/b

Figure 2.1.7: Performance summary and comparison.

978-1-61284-302-5/11/$26.00